Available online at www.sciencedirect.com
SCIENCE DIRECT®
Journal of Solid State Chemistry 179 (2006) 62–69
JOURNAL OF SOLID STATE CHEMISTRY
www.elsevier.com/locate/jssc

Visible-light-driven photocatalyst of Bi_2WO_6 nanoparticles prepared via amorphous complex precursor and photocatalytic properties

Shicheng Zhang[1], Chuan Zhang, Yi Man, Yongfa Zhu*

Department of Chemistry, Tsinghua University, Beijing 100084, PR China

Received 14 August 2005; received in revised form 21 September 2005; accepted 24 September 2005
Available online 26 October 2005

Abstract

The visible-light-driven photocatalyst Bi_2WO_6 nanoparticles have been prepared by calcining amorphous complex precursor at a relatively low temperature of above 450 °C. The effects of calcination temperature and time on the structures and properties of Bi_2WO_6 nanoparticles have been investigated in detail. The photocatalytic activity of the Bi_2WO_6 powders were evaluated by degradation of RhB molecules in water under visible light irradiation ($\lambda > 400$ nm). The results showed that the particle size and grain size of Bi_2WO_6 increased with the calcination temperature and time. The photocatalytic activity of the best sample was about 8.8 times higher than that of the sample prepared by traditional solid state reaction and the photo-degradations was a zero-order reaction. The best route to enhance the photocatalytic activity of Bi_2WO_6 was to prepare the sample at a lower temperature for a longer time, due to the samples with better crystallization and smaller particle size.

Keywords: Bi_2WO_6; Photocatalysis; Visible light; Amorphous complex precursor; RhB

1. Introduction

Since the photoinduced decomposition of water on a TiO_2 electrode was discovered by Honda et al. [1], semiconductor-based photocatalysis has attracted great interest for their application in water splitting [2,3], destruction of chemical contaminants [4], etc. TiO_2 has by far the most popular one for its higher photocatalytic activity, good photostability, non-toxicity, and low price. But a major drawback of TiO_2 is the large bandgap of 3.2 eV, so wavelengths below 400 nm are necessary for excitation, which limits the usage efficiency of solar energy. In recent years, some complex oxides have been found to have the visible light driven catalytic activity with the perovskite or monoclinic structure, such as $BiVO_4$ [5,6], $In_{1-x}Ni_xTaO_4$ ($x = 0-0.2$) [7], $RbLnTa_2O_7$ (Ln = La, Pr, Nd, and Sm) [8], $MIn_{0.5}Nb_{0.5}O_3$ (M = Ca, Sr, and Ba) [9], $CaIn_2O_4$ [10], etc.

Bi_2WO_6 is one of the simplest Aurivillius oxides with $n = 1$, which possess layered structure with the perovskite-like slab of WO_6 [11]. Dielectric, ion conductive, luminescent and catalytic properties of this material have attracted attention. Recently, it has also been reported that Bi_2WO_6 is a good photocatalyst for water splitting and photodegradation of organic compounds under visible light irradiation [12,13]. However, all Bi_2WO_6 samples were prepared by solid-state reaction in their work, which it was essential to perform at high temperature, and the photocatalytic activities were not high due to large crystal and low surface area. Some new attempts have been done about synthesis of Bi_2WO_6 by using hydrothermal method to obtain high surface area [14–17].

Here, we report another new method for preparation of Bi_2WO_6 nanoparticles from amorphous precursor. This kind of method for preparation of nanoparticles from amorphous complex precursor has been used in preparation of complex oxides powders or films due to their luminescent, ferroelectric, magnetic, catalytic, and electric

*Corresponding author.
E-mail addresses: zhangsc@fudan.edu.cn (S. Zhang), zhuyf@mail.tsinghua.edu.cn (Y. Zhu).
[1]Current address: Shicheng Zhang, Department of Envionmental Science and Engineering, Fudan University, Shanghai 200433, China.

0022-4596/$ - see front matter © 2005 Elsevier Inc. All rights reserved.
doi:10.1016/j.jssc.2005.09.041

properties [18–21]. The advantages of this method are easy to form the complex oxide at relative low calcination temperature, easy to dope, and suitable for fabrication of the complex oxide films by dip-coating or spin-coating technique. But to our knowledge, still no literature reports the preparation of photocatalysts by using this kind of method. In this paper, the visible-light-driven photocatalyst Bi_2WO_6 was obtained from amorphous precursor. The formation process and the visible light photocatalytic properties of Bi_2WO_6 have been investigated in detail.

2. Experimental section

2.1. Preparation of Bi_2WO_6 nanoparticles

The preparation procedure of Bi_2WO_6 nanoparticles includes preparation of the precursor and the subsequent calcination. Detailed procedures were described below.

The 0.02 mol of diethylenetriaminepentaacetic acid (H_5DTPA) and 7.5 mL stronger ammonia water (about 13.0 mol L^{-1}) were added in 200 mL hot distilled water. After dissolution, the 0.005 mol Bi_2O_3 and 0.00042 mol $5(NH_4)_2O \cdot 12WO_3 \cdot 5H_2O$ powders were added in. It was stirred and heated at about 80 °C to promote the dissolution and reaction until the mixture became a colorless transparent solution. After being vaporized slowly at 80 °C, the solution became a piece of transparent glass-like material used as the precursor.

The Bi_2WO_6 nanoparticles were obtained by decomposing the precursor in air. At first, the temperature was raised to 350 °C at a slow heating rate (3 °C min^{-1}). Second, keep the sample at this temperature for 4 h to promote the decomposition of organic components. At last, the temperature increased to various pre-set temperatures and was maintained for a definite period of time to promote the formation of Bi_2WO_6.

Meanwhile Bi_2WO_6 were synthesized by traditional solid-state reaction according to Ref. [12] for comparison with the nanoparticles.

2.2. Sample characterization

X-ray diffraction (XRD) experiments were carried out in Bruker D8 Advance diffractometer with Cu$K\alpha$ radiation. The morphology of the samples was measured by using transmission electron microscopy (TEM) and scanning electron microscopy (SEM). TEM was performed by using a JEOL JEM-1200EX instrument with the accelerating voltage of the electron beam of 120 kV. SEM was taken using a KY2800 electron microscope (Scientific Instrumental Plant of Chinese Academy of Sciences). Thermogravimetry (TG) and differential thermal analysis (DTA) analyses were performed on a Du Pont Universal V2.6D thermal analyzer. The atmosphere was air and the heating rate was 10 °C min^{-1}. UV-Vis diffuse reflectance spectrums (DRS) of the samples were measured by using Hitachi U-3010 UV-Vis spectrophotometer. The surface area of the photocatalysts was determined by N_2 adsorption–desorption measurement (ASAP 2010 V5.02H) on nitrogen adsorption at −196 °C after the pretreatment at 300 °C for 2 h.

2.3. Photocatalytic reactions

The visible light photocatalytic activities of Bi_2WO_6 nanoparticles were valued by the decomposition of rhodamine B (RhB) in water. The optical system for the photocatalytic reaction was composed of a 500-W Xe arc lamp and a cutoff filter ($\lambda > 400$ nm). The average light intensity was 31 mW cm^{-2}. The irradiation area was approximately 40 cm^2. The radiant flux was measured with a power meter from Institute of Electric Light Source (Beijing). The photocatalytic reaction procedures are similar to that in the reference [22]. RhB solutions (100 mL, 10^{-5} mol L^{-1}) containing 0.1 g of Bi_2WO_6 nanoparticles were put in a glass beaker. Before the light was turned on, the solution was first ultrasonicated for 10 min, and then stirred for 30 min to ensure equilibrium between the catalyst and the solution. 3 mL of samples were taken at given time intervals and separated through centrifugation (4000 rpm, 10 min). The supernatants were analyzed by recording variations of the absorption band maximum (553 nm) in the UV-Vis spectra of RhB by using a U-3010 spectrophotometer (Hitachi). The extent of adsorption of RhB on Bi_2WO_6 was determined by the difference in the concentration of RhB between the original solution and the filtrate of the RhB/Bi_2WO_6 dispersions.

3. Results and discussions

3.1. Preparation and characterization of Bi_2WO_6 photocatalysts

It is well known that the crystallinity and the particle size of the photocatalyst are two important factors influencing the photocatalytic activity. The higher the crystalline quality, the smaller is the amount of defects. The defects operate as trapping and recombination centers between photogenerated electrons and holes, resulting in a decrease in the photocatalytic activity. Therefore, a high degree of crystallinity is required for photocatalysts. At the same time, the smaller the particle size is, the bigger the surface area is, and the more the active sites are, that can lead to higher photocatalytic activity.

XRD, TEM, SEM, and BET were used to investigate the crystal structure, morphology, particle size, and surface area of the as-prepared samples. In order to investigating the formation process of the Bi_2WO_6 nanoparticles, the TG and DTA spectra were used to detect the decomposition process of the precursor firstly.

Fig. 1 shows the TG and DTA spectra of the precursor. The TG curve indicated that the increase of temperature resulted in four different regions of weight loss. Based on the quantitative calculation, the formula of the precursor

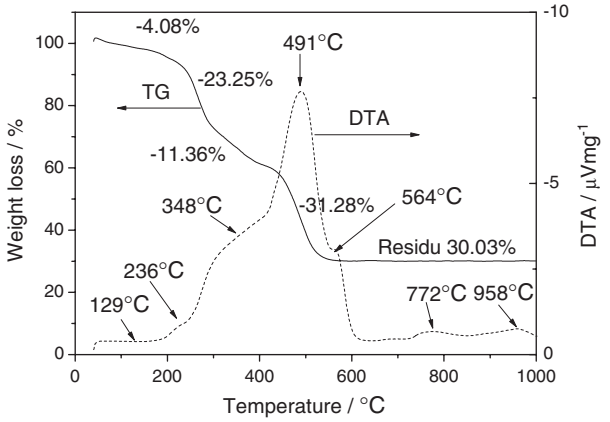

Fig. 1. TG and DTA analysis of $(NH_4)_4Bi_2W(DTPA)_4 \cdot 5H_2O$ precursor.

could be shown as $(NH_4)_4Bi_2W(DTPA)_4 \cdot 5H_2O$. The theoretical water contents and the residue (corresponding to Bi_2WO_6) are 3.88% and 30.11%, which agree pretty well with the experimental values (the water contents of 4.08% and the residue of 30.03%). The thermal decomposition processes could be distinguished as followings, which was similar to that of LaNi (DTPA) $6H_2O$ for preparation of $LaNiO_3$ [21] and that of polyaminocarboxylate for preparation of Bi–La and Bi–Pr oxides [18,23]. The weight loss region from 45 to 195 °C was caused by the loss of coordinated water. The region from 195 to 301 °C resulted from the decomposition of the organic group, including the decomposition of hydrocarbon, amino-group organic compounds. The region from 301 to 401 °C resulted from the decomposition of carboxyl tungsten group and the region from 401 to 595 °C resulted from the decomposition of carboxyl bismuth group. All organic components could have been eliminated at 600 °C because there was no future weight loss region.

On the DTA curve one endothermic and six exothermic peaks were observed. The little endothermic peak at 129 °C was attributed to the loss of the coordinated water. The peak at 236 °C was produced by the burning of hydrocarbon and amino-group. The peak at 348 °C was produced by the decomposition of carboxyl tungsten group. The peak at 491 °C was very strong, which contained both exothermic contribution from the decomposition of carboxyl bismuth group and the formation of Bi_2WO_6 complicated oxide. Because the exothermic heat of carboxyl group was small, most exothermic heat came from the formation of tungstate. The shoulder peak at 564 °C resulted from the crystallization of Bi_2WO_6. The peaks at 772 and 958 °C were produced by the phase transition of Bi_2WO_6, which had been investigated in the literature [24]. The above results suggest that Bi_2WO_6 can be formed below 600 °C by decomposing an amorphous complex.

The XRD results showed good agreement with the TG and DTA spectra. Fig. 2 showed the XRD patterns of decomposition species from the precursor under different

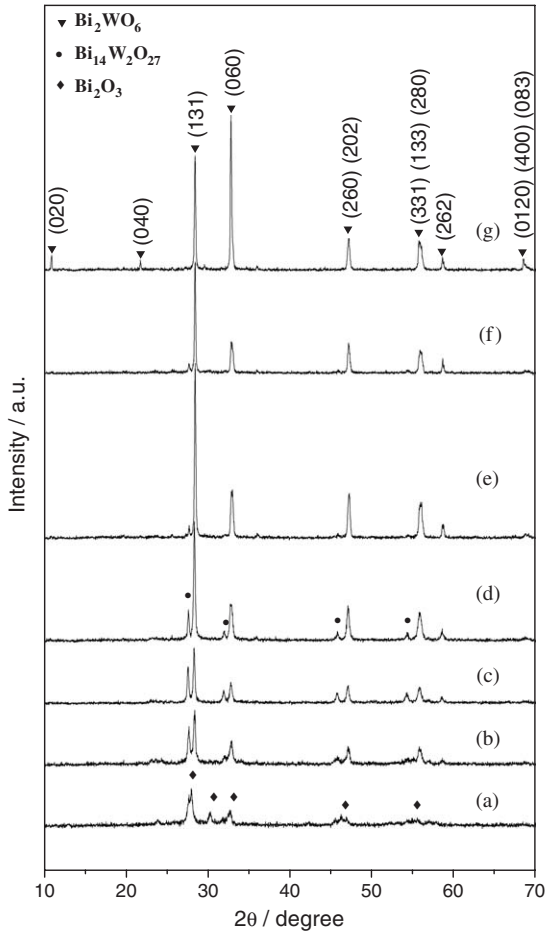

Fig. 2. XRD patterns of as-prepared powders obtained under different calcination temperature: (a) 400 °C; (b) 450 °C; (c) 500 °C; (d) 550 °C; (e) 600 °C; (f) 700 °C; (g) 800 °C.

calcination temperature for 4 h. XRD results showed that the Bi_2WO_6 phase did not form when the calcination temperature was 400 °C. After the calcination temperature increased to 450 °C, several broad peaks of Bi_2WO_6 and $Bi_{14}W_2O_{27}$ appeared, implying the formation of Bi_2WO_6 crystalline phase with some impurities of $Bi_{14}W_2O_{27}$. From the TG-DTA results (Fig. 1), at 450 °C, the carboxyl bismuth group and the carboxyl tungsten group have both started to decompose, and the organic components have not been eliminated completely. Also, from the phase diagram of Bi_2O_3–WO_3 [25], the Bi_2WO_6 phase can be got at relatively lower temperature with other impurities. So, it can be concluded that the Bi_2WO_6 phase can be got at the decomposition process of complex precursor above 450 °C. With the increase of the calcination temperature, the intensity of diffraction of the Bi_2WO_6 phase increased and that of $Bi_{14}W_2O_{27}$ phase decreased gradually. The pure Bi_2WO_6 phase can be got above 600 °C. The peaks of Bi_2WO_6 became sharper with the calcination temperature, which implied the crystalline of Bi_2WO_6 became more perfect. At 800 °C, the peaks of (020), (040), and (060) were enhanced, which implied that the crystallization of Bi_2WO_6 had the layered structure paralleling to the (010) face.

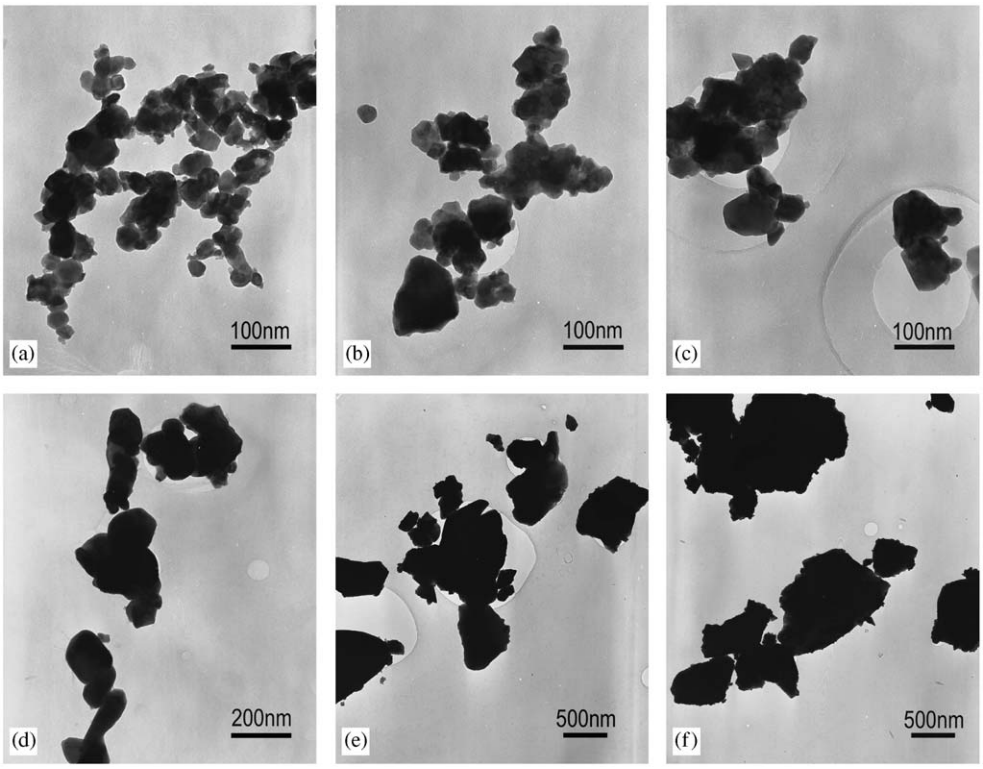

Fig. 3. TEM morphologies of as-prepared powders obtained under different calcination temperature: (a) 450 °C; (b) 500 °C; (c) 550 °C; (d) 600 °C; (e) 700 °C; (f) 800 °C.

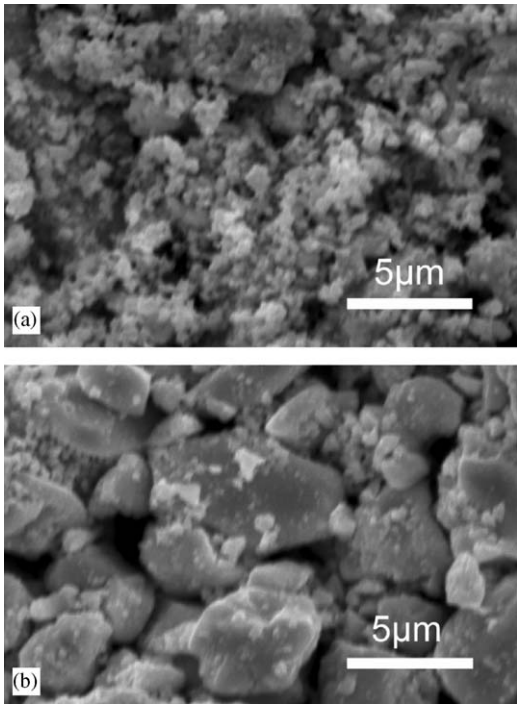

Fig. 4. SEM morphologies of as-prepared powders obtained under different calcination temperature: (a) 600 °C; (b) 800 °C.

The morphology and the particle size of Bi_2WO_6 were modified by changing the calcination temperature, which could be found from the TEM, SEM, and BET results (Figs. 3 and 4). Fig. 3 showed that the particle size was homogenous and fairly small (about 30 nm) when the sample was obtained at a low calcination temperature such as 450 °C. The particle size grew quickly after the sample was calcined at a higher temperature. The particle size was much larger (about 100–200 nm) after the sample was calcined at 600 °C for 4 h and even larger (about several hundred nanometers to several micrometers) when the temperature was 800 °C. The SEM images showed the aggregation and sintering between the particles more distinctly (Fig. 4) when the temperature increased. The BET surface area of the Bi_2WO_6 nanoparticles prepared at 500 °C was about 8.6 $m^2 g^{-1}$, which was over ten times that of the sample prepared by traditional solid state reaction (about 0.64 $m^2 g^{-1}$, [12]).

We have also compared the grain size from XRD using Scherrer methods [21] and the particle size counted from TEM images (Fig. 5). With the increase of the calcination temperature, the particle size increased dramatically, especially under the temperature bigger than 600 °C, and the deviation of the particle size increased. But the grain size increased slightly. This means that the big particles were composed of several grains. From the TEM and SEM images (Figs. 3 and 4), we can not distinguish the grain boundary. So we can conclude that the big particles were formed by sintering several grains into a big one, and were not the simply soft aggregate of grains.

The influences of calcination time on the phase structure and the morphology of Bi_2WO_6 were shown in Figs. 6 and 7.

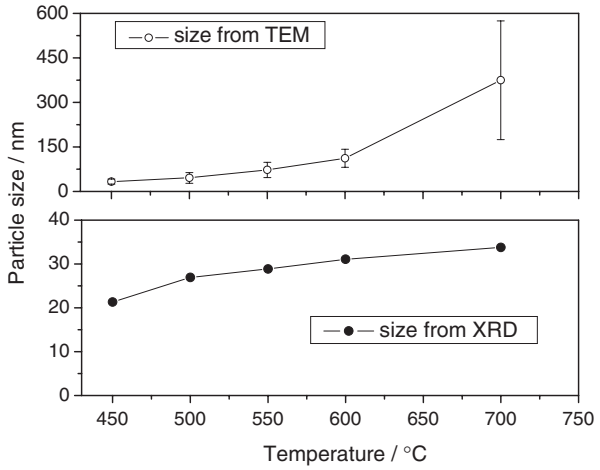

Fig. 5. Influence of calcination temperature on the size of Bi_2WO_6 nanoparticles determined from TEM and XRD.

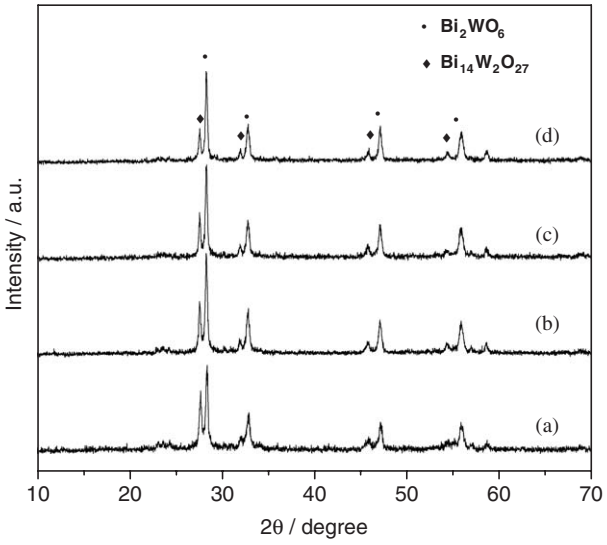

Fig. 6. XRD patterns of as-prepared powders obtained by calcining at 450 °C for different time: (a) 4 h; (b) 12 h; (c) 24 h; (d) 48 h.

Fig. 8 showed the particle size (counted from TEM images) and grain size (calculated from XRD) of Bi_2WO_6 with the calcination time. The precursors were calcined at 450 °C for 4, 12, 24, and 48 h, respectively. With the increase of calcination time, the intensity of diffraction of the Bi_2WO_6 phase increased and that of $Bi_{14}W_2O_{27}$ phase decreased gradually. The crystal structure of Bi_2WO_6 changed little when calcination time was prolonged, indicating that the calcination time had less effect on the crystallization process. Meanwhile, from Figs. 7 and 8, we can fond that, when the calcination time increased, the particle size changed little (from 34 to 45 nm), but the surface of the particles was more regular, which means the higher crystallinity of Bi_2WO_6. When the calcination time prolongs to 48 h, some particles interconnected with each other and interfused to the bigger

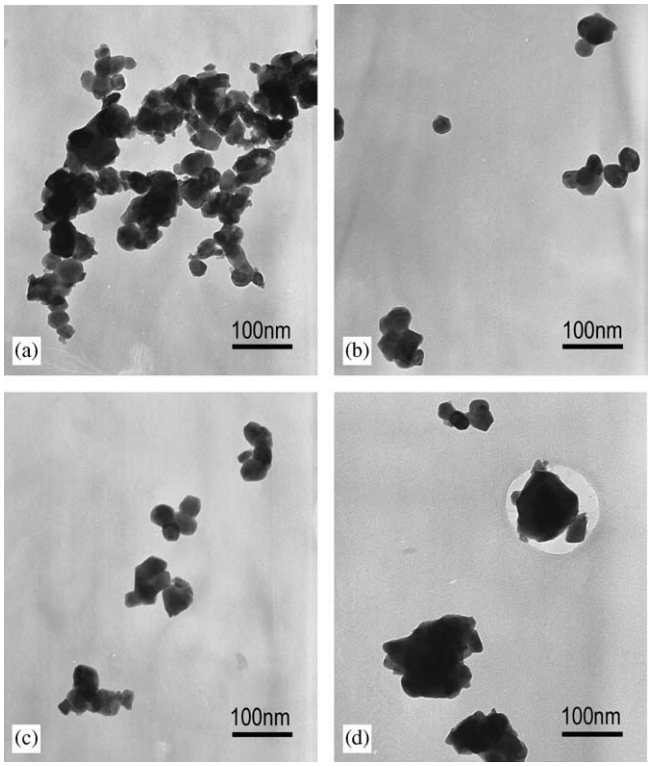

Fig. 7. TEM morphologies of as-prepared powders obtained under different calcination time: (a) 4 h; (b) 12 h; (c) 24 h; (d) 48 h.

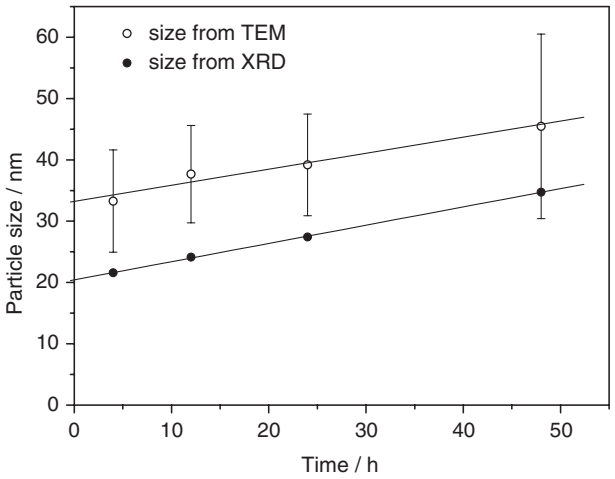

Fig. 8. Influence of calcination time on the size of Bi_2WO_6 nanoparticles determined from TEM and XRD.

particles with the size of 50–100 nm, and lead to the broad distribution of the particle size. From Fig. 8, we can also find that the particle size and the grain size both increase linearly with the calcination time. The particle size is slightly bigger than the grain size, which means that each particle was one grain, or sintered from two grains.

The above results indicated that Bi_2WO_6 crystalline phase could be formed at a relatively low temperature and for a short time by using an amorphous complex as a

precursor. For the semiconductor photocatalysts, it is essential to get higher crystallinity and higher surface area. In order to get this goal, the Bi_2WO_6 nanoparticles should be obtained a relatively low temperature and a longer calcination time. The lower preparation temperature (about 450 °C), and the higher viscosity of the amorphous complex precursor make this kind of method is suitable to prepare the Bi_2WO_6 photocatalytic films on ITO glass substrate by dip-coating technique. The detailed investigation about the preparation, photocatalytic properties and photoelectrochemical properties of the Bi_2WO_6 films will be shown in another paper.

3.2. Photophysical and photocatalytic properties

Diffuse reflectance spectra of the Bi_2WO_6 powders prepared under different conditions are shown in Fig. 9. The absorption edges observed in a visible light region did not have much difference between the Bi_2WO_6 powders prepared under different calcination temperature and different calcination time. The diffuse reflectance spectra of the Bi_2WO_6 powders prepared at low temperature and short time have a tail at the absorption edge. It suggests the formation of surface states and impurity levels, which can also be confirmed by the XRD patterns (Figs. 2 and 6).

For a crystalline semiconductor, it is known that the optical absorption near the band edge follows the equation

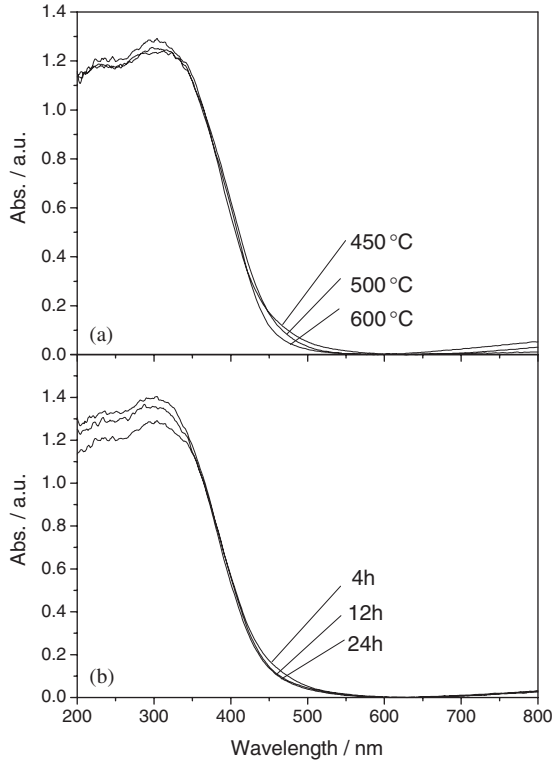

Fig. 9. UV-Vis diffuse reflectance spectra of the Bi_2WO_6 powders prepared under different calcination temperature (a) and different calcination time (b).

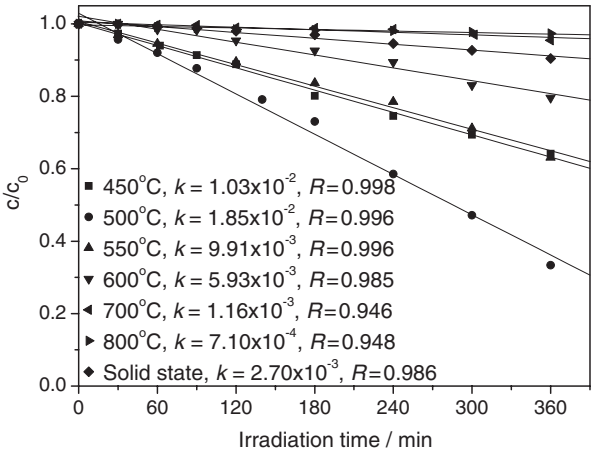

Fig. 10. Photocatalytic degradation of RhB (10^{-5} mol L^{-1}) under visible light (wavelength >400 nm) at room temperature in air for 360 min over Bi_2WO_6 particles prepared under different calcination temperature. Also shows the values of the photodegradation rate constant k ($\times 10^{-6}$ mol L^{-1} min^{-1}) and the linearly dependent coefficient R.

[26–28]:

$$ahv = A(hv - E_g)^{n/2} \quad (1)$$

in which a, v, A, n, and E_g are absorption coefficient, light frequency, proportionality constant, an integer ($n = 1, 2, 4$, and 6), and band gap, respectively. The values of n and E_g were determined by the following steps: first, plot ln(ahv) vs. ln($hv-E_g$), using an approximate value of E_g, and then determine the value of n with the slope of the straightest line near the band edge; second, plot $(ahv)^{2/n}$ vs. hv and then evaluate the band gap E_g by extrapolating the straightest line to the hv axis intercept. The value of n for Bi_2WO_6 was determined as 2 from Fig. 9. This means that the optical transitions for the oxide are directly forbidden. The value of the band gap for Bi_2WO_6 obtained under different conditions was about 2.75 eV, which is similar to the value in literatures [12,13].

The photocatalytic activity of the Bi_2WO_6 nanoparticles was evaluated by degradation of RhB molecules in water. Figs. 10 and 11 showed time profiles of C/C_0 under visible light irradiation ($\lambda > 400$ nm), where C was the concentration of RhB at the irradiation time t and C_0 was the concentration in the adsorption equilibrium on Bi_2WO_6 before irradiation. The C/C_0 linearly decreased, which meaned the photodegradation of RhB over Bi_2WO_6 could be described as zero-order reaction [6]. Figs. 10 and 11 also showed the values of the photodegradation rate constant k ($\times 10^{-6}$ mol L^{-1} min^{-1}) and the linearly dependent coefficient R. The photocatalytic activity of Bi_2WO_6 can be evaluated by using the value of k, i.e. the bigger the value of k, the higher the photocatalytic activity. For the samples prepared at lower temperatures, the coefficients R were bigger than 0.99, and showed good linear dependence relation. For the samples prepared at higher temperatures (700 and 800 °C), their particle size were too big to get a

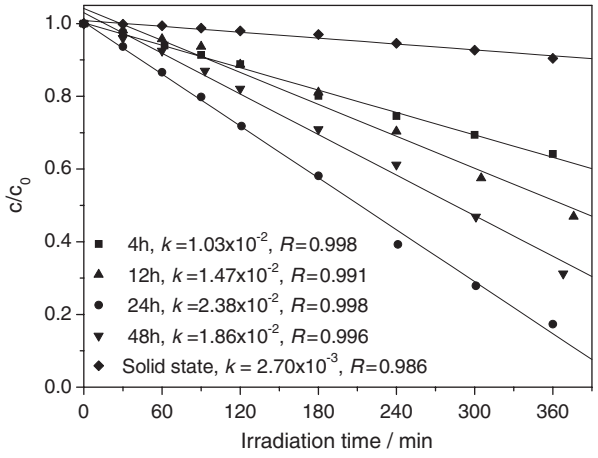

Fig. 11. Photocatalytic degradation of RhB (10^{-5} mol L^{-1}) under visible light (wavelength >400 nm) at room temperature in air for 360 min over Bi_2WO_6 particles prepared under different calcination time. Also shows the values of t the photodegradation rate constant k ($\times 10^{-6}$ mol L^{-1} min^{-1}) and the linearly dependent coefficient R.

homogeneous Bi_2WO_6 suspension in water. So that the errors of the measurements increased and the linear dependence coefficient decreased. But the value of R still had some reference to the comparison of the photocatalytic activity.

The photocatalytic activities of the photocatalysts were highly corresponding to their surface structures and crystallinity. From Fig. 10, we can find that with the increase of calcination temperature, the photocatalytic activities of Bi_2WO_6 increased firstly, and then decreased under the calcination temperature of higher than 500 °C. From the TEM (Fig. 3) and XRD (Fig. 2) results, with the increase of the calcination temperature, the crystallinity of Bi_2WO_6 increased, and the contents of the impurities decreased, which benefit to the photocatalytic properties. But, the particle size increased also, which lead to the lower specific surface area and lower absorptive capacity of RhB on the surface of Bi_2WO_6 particles, and then the lower photocatalytic activity. So the best method to enhance the photocatalytic activity of Bi_2WO_6 is to calcine it under a lower temperature for a longer time.

Fig. 11 shows the photocatalytic activities of the Bi_2WO_6 particles obtained by calcination at 450 °C for different time. With the increase of calcination time, the photocatalytic activity increased, and the highest photocatalytic activities was got at the time of 24 h. This is corresponding to the TEM (Fig. 7) and XRD (Fig. 6) results. Prolonging the calcination time is an effective route to promote the crystallization of Bi_2WO_6 particles, and then get a higher photocatalytic activity. But the too long of the calcination time still can lead to the increase of the particle size, and lower the photocatalytic activity.

The photocatalytic activities of most samples were higher than that of the sample prepared by traditional solid state reaction (Figs. 10 and 11). The rate constant k of the best sample in our experiments is $2.38 \times \times 10^{-2}$, which is about 8.8 times that of the sample prepared by traditional solid state reaction (2.70×10^{-3}). Means the photocatalytic activity of the best-quality Bi_2WO_6 nanoparticles was about 8.8 times higher.

4. Conclusions

In summary, Bi_2WO_6 nanoparticles have been obtained by calcining amorphous complex precursor at a relatively low temperature of above 450 °C, which is suitable for preparation of the Bi_2WO_6 photocatalytic films on ITO glass by dip-coating technique. The crystallinity, particle size, morphology, and photocatalytic activity of the Bi_2WO_6 nanoparticles can be modified easily by changing the calcination temperature and time. The Bi_2WO_6 nanoparticles showed higher photocatalytic activities under visible light irradiation ($\lambda > 400$ nm), with the photocatalytic activity of about 8.8 times higher than that of the sample prepared by traditional solid state reaction. This method has the potential use in preparation of other complex oxide photocatalysts powders and thin film photoelectrodes.

Acknowledgments

This work was partly supported by Chinese National Science Foundation (20433010), Trans-Century Training Program Foundation for the Talents by the Ministry of Education, P.R.C., the Excellent Young Teacher Program of MOE, P.R.C., and the China Postdoctoral Science Foundation.

References

[1] K. Honda, A. Fujishima, Nature 238 (1972) 37.
[2] A. Kudo, Catal. Surv. Asia 7 (2003) 31.
[3] T. Takata, A. Tanaka, M. Hara, J.N. Kondo, K. Domen, Catal. Today 44 (1998) 17.
[4] M.R. Hoffmann, S.T. Martin, W. Choi, D.W. Bahnemannt, Chem. Rev. 95 (1995) 69.
[5] A. Kudo, K. Omori, H. Kato, J. Am. Chem. Soc. 121 (1999) 11459.
[6] S. Kohtani, M. Koshiko, A. Kudo, K. Tokumura, Y. Ishigaki, A. Toriba, K. Hayakawa, R. Nakagaki, Appl. Catal. B 46 (2003) 573.
[7] Z.G. Zou, J.H. Ye, K. Sayama, H. Arakawa, Nature 414 (2001) 625.
[8] M. Machida, J. Yabunaka, T. Kijima, Chem. Mater. 12 (2000) 812.
[9] J. Yin, Z.G. Zou, J.H. Ye, J. Phys. Chem. B 107 (2003) 61.
[10] J.W. Tang, Z.G. Zou, J.H. Ye, Chem. Mater. 16 (2004) 1644.
[11] J. Ricote, L. Pardo, A. Castro, P. Millan, J. Solid State Chem. 160 (2001) 54.
[12] J.W. Tang, Z.G. Zou, J.H. Ye, Catal. Lett. 92 (2004) 53.
[13] A. Kudo, S. Hijii, Chem. Lett. (1999) 1103.
[14] Y. Shi, S. Feng, C. Cao, Mater. Lett. 44 (2000) 215.
[15] C. Zhang, Y.F. Zhu, Chem. Mater. 17 (2005) 3537.
[16] H.B. Fu, C.S. Pan, W.Q. Yao, Y.F. Zhu, J. Phys. Chem. B, in press.
[17] J.G. Yua, J.F. Xiong, B. Cheng, Y. Yu, J.B. Wang, J. Solid State Chem. 178 (2005) 1968.
[18] H. Wullens, D. Leroy, M. Devillers, Int. J. Inorg. Mater. 3 (2001) 309.
[19] C. Zhang, L. Wang, L.P. Cui, Y.F. Zhu, J. Crystal Growth 255 (2003) 317.

[20] Y.F. Zhu, R.Q. Tan, J. Feng, S.S. Ji, L.L. Cao, Appl. Catal. A 209 (2001) 71.
[21] H. Wang, Y.F. Zhu, P. Liu, W.Q. Yao, J. Mater. Sci. 38 (2003) 1939.
[22] J.C. Zhao, T.X. Wu, K.Q. Wu, K. Oikawa, H. Hidaka, N. Serpone, Environ. Sci. Technol. 32 (1998) 2394.
[23] H. Wullens, N. Bodart, M. Devillers, J. Solid State Chem. 167 (2002) 494.
[24] V.K. Yanovskii, V.I. Voronkova, Phys. Stat. Sol. (a) 93 (1986) 57.
[25] T. Suzuki, T. Yamazaki, E. Hosaka, H. Yoshioka, J. Mater. Sci. 20 (1985) 4155.
[26] M.A. Butler, J. Appl. Phys. 48 (1977) 1914.
[27] J. Yin, Z.G. Zou, J.H. Ye, J. Phys. Chem. B 107 (2003) 4936.
[28] J.W. Tang, Z.G. Zou, J.H. Ye, J. Phys. Chem. B 107 (2003) 14265.